Teranishi *et al. J Wood Sci* (2021) 67:41
https://doi.org/10.1186/s10086-021-01973-9

Journal of Wood Science

NOTE

Open Access

Nonlinear finite-element analysis of embedment behavior of metal washer in bolted timber joints

Masaki Teranishi[1*], Doppo Matsubara[2], Yoshiaki Wakashima[3], Hidemaru Shimizu[4] and Akihisa Kitamori[5]

Abstract

The pretensioning force in bolted joints enhances the lateral strength of the connections, and causes the embedment of metal washers into wood. Despite the significance of embedment behavior in the design of bolted joints, its mechanism has yet to be fully understood. In this study, the mechanism of the embedment of a metal washer into wood along the radial direction was examined through three-dimensional nonlinear finite-element analysis (FEA). The FEA results were validated by comparing them with experimental results for nine metal washers with different geometries. Moreover, the sensitivity of embedment stiffness and yield load to wooden material constants was also investigated. The numerical results showed good qualitative and quantitative agreement with the experimental results. In addition, the embedment stiffness and yield load were sensitive to the yield stress and Young's modulus of wood in the radial and tangential directions. The determination of these mechanical properties of wood through material testing is important for reproducing the behavior of the embedment of a metal washer into wood and accurately estimating the yield load and initial stiffness using FEA. This will play a significant role in designing bolted joints.

Keywords: Finite-element analysis, Contact problem, Pretensioned bolted joint, Embedment behavior, Metal washer, Sensitivity analysis

Introduction

Timber connections with dowel-type fasteners are frequently used as load-carrying parts between members in timber structures. The appropriate design of dowel-type fasteners plays a significant role in increasing the ductility of timber connections [1]. The load–slip characteristics of laterally loaded dowel-type joints have been experimentally and numerically investigated [2–7].

The axial force on laterally loaded dowel-type fasteners contributes to strengthening the lateral strength of connections; this is referred to as the rope effect. This effect becomes particularly significant in slender dowel-type fasteners. The rope effect improves the load-carrying capacity of bolted joints under monotonic loading [8] and cyclic loading [9, 10] and the load-carrying capacity of timber-to-timber connections [5].

The pretensioning force on bolted joints causes the embedment of steel plates into wood. Thus, the embedment mechanism plays a significant role in designing bolted joints. The theory of beams on elastic foundation was applied to the embedment of metal washers into wood; the proposed method could estimate embedment stiffness and yield resistance [11]. Three-dimensional finite-element analysis (FEA) of embedment has been performed, and good agreement was qualitatively obtained between the embedment load–displacement curves obtained via FEA and an embedment test [12]. However, the aforementioned studies did not fully address the mechanism of the initiation and development of the plastic deformation of wood. The elucidation of this mechanism is necessary to evaluate the strength

*Correspondence: masaki_t@eng.niigata-u.ac.jp
[1] Niigata University, 8050, Ikarashi 2-no-cho, Nishi-ku, Niigata 950-2181, Japan
Full list of author information is available at the end of the article

of pretensioned bolted joints accurately. FEA is a useful tool for the investigation of this mechanism; its results depend greatly on the elastic modulus and yield stress of wood. The mechanical properties of wood vary largely among specimens. However, the sensitivity of the embedment mechanism to the mechanical properties of wood to verify the reliability of FEA for designing pretensioned bolted joints have been rarely studied.

In this study, the mechanism of the embedment of metal washers into wood was investigated through three-dimensional nonlinear FEA, where a bolt, metal washer, and wood were finely discretized. The FEA results were validated by comparing them with experimental results. Moreover, FEA was carried out with intentionally changed material constants to investigate the sensitivity of embedment stiffness and the yield load to wooden material constants.

Materials and methods

Experimental conditions

The embedment behavior of the metal washers into wood was investigated by Matsubara et al. [11] through embedment tests. This section provides an overview of the experiment, which is described in detail in their paper. The schematic of the embedment test setup is shown in Fig. 1. A square metal washer and nut were set on the wood. The nut was pressed vertically; then, the metal washer was embedded into the wood. A bolt hole with a diameter of 13.0 mm was created at the center of the wood. The lengths of the wood in the longitudinal, radial, and tangential directions were 130, 29, and 99 mm, respectively. Square washers with three different side lengths (40, 60, and 80 mm) and three different thicknesses (2.3, 4.5, and 6.0 mm) were employed. The embedment load was measured using a load cell, and the embedment displacement was measured by the vertical displacement of the crosshead. The radial direction of wood was parallel to the loading direction.

Numerical conditions

A finite-element (FE) model was created using Abaqus/CAE. Figure 2 shows the three-dimensional FE model of the embedment test system with the square metal washer of thickness 2.3 mm and a side length of 40 mm. A quarter FE model was used by considering mechanical symmetry, where symmetric planes were created on the bolt, metal washer, and wood. The bolt, metal washer, and wood were discretized using the 20-node brick element (C3D20). The number of nodes and elements in all FE models is listed in Table 1. It should

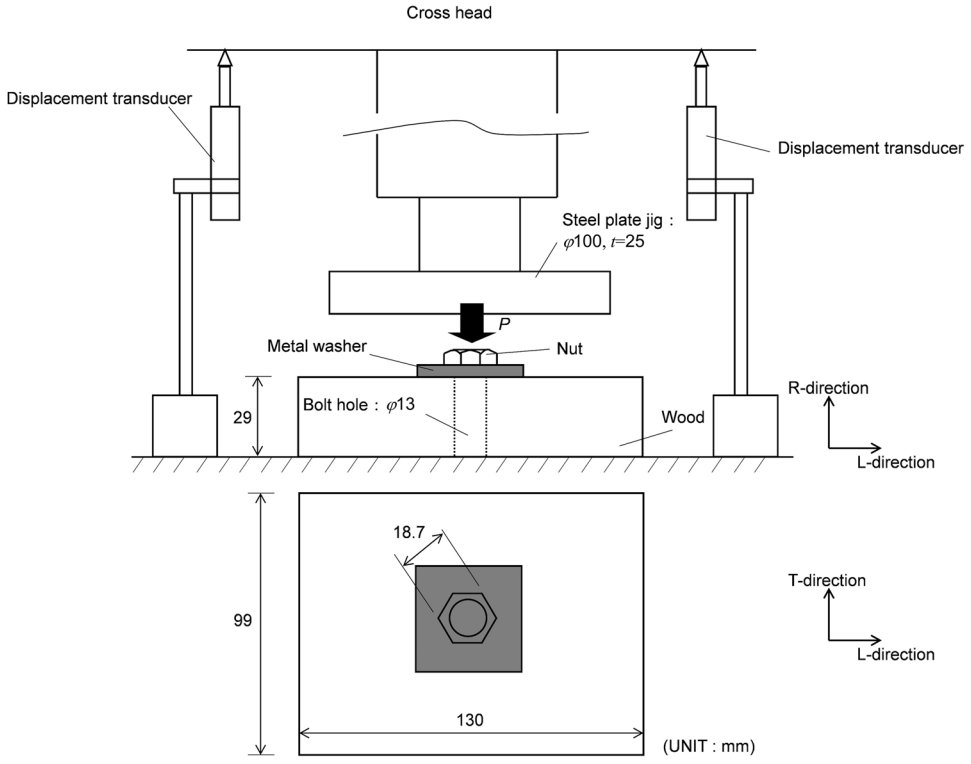

Fig. 1 Schematic of apparatus for embedment test (L: longitudinal, T: tangential, R: radial)

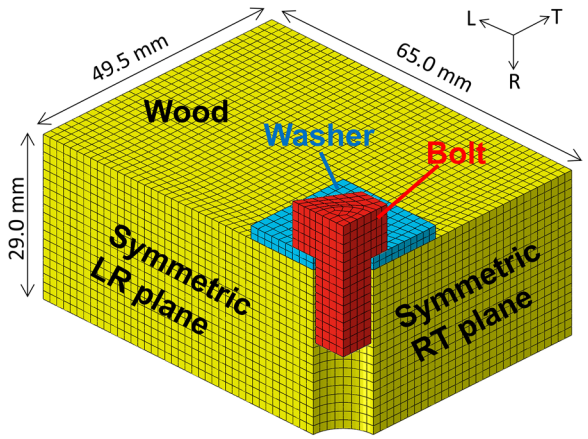

Fig. 2 Finite-element model of metal washer with a thickness of 2.3 mm and a side length of 40 mm (L: longitudinal, T: tangential, R: radial)

Table 1 Number of nodes and elements in each finite-element model

Metal washer		Model	Num. of nodes	Num. of elements
Side length [mm]	Thickness [mm]			
40	2.3	S40T2.3	116,403	26,640
	4.5	S40T4.5	117,036	26,779
	6.0	S40T6	117,669	26,918
60	2.3	S60T2.3	118,902	27,074
	4.5	S60T4.5	120,445	27,430
	6.0	S60T6	121,988	27,786
80	2.3	S80T2.3	122,446	27,698
	4.5	S80T4.5	125,279	28,366
	6.0	S80T6	128,112	29,034

be noted that the influence of element size was investigated by comparison among numerical results with various element sizes, and the sufficiently fine mesh was employed in the FE model. The FE models were identified by the thickness and side length of the metal washer, e.g., the model of the washer with a side length of 40 mm and a thickness of 2.3 mm thickness was named S40T2.3.

The bottom of the wood was fixed in all directions. The symmetric plane was fixed in the direction perpendicular to itself. The surface-to-surface contact condition was imposed on the bolt-to-washer and washer-to-wood interfaces, where the horizontal friction coefficients were 0.4 and 0.3, respectively [8, 13]. The augmented Lagrangian method was employed on the contact surface. In this method, penalty stiffness is used during the augmentation iteration to improve the accuracy of approximation. The penalty stiffness was set as 205000 MPa.

The metal washer and bolt were assumed as isotropic materials with isotropic linear elasticity, the von Mises yield criterion, and perfect elastoplasticity [14]. The Young's modulus, Poisson's ratio, and yield stress for the metal washer and bolt were denoted as E, ν, and σ^y, respectively. Unlike the metal washer and bolt, the wood was assumed as an orthotropic material with orthogonal linear elasticity, Hill's anisotropic yield criterion, and perfect elastoplasticity [15, 16]. The Hill's anisotropic yield criterion has been frequently used in wooden material [6, 12, 17]. Subscripts L, R, and T were used to denote the properties of the wood in the longitudinal, radial, and tangential directions, respectively. For example, the Young's moduli of the wood in the longitudinal, radial, and tangential directions were denoted as E_L, E_R, and E_T, respectively. Hill's anisotropic yield criterion used for the wood was as follows [16]:

$$f = \sqrt{F(\sigma_{RR} - \sigma_{TT})^2 + G(\sigma_{TT} - \sigma_{LL})^2 + H(\sigma_{LL} - \sigma_{RR})^2 + 2L\sigma_{RT}^2 + 2M\sigma_{TL}^2 + 2N\sigma_{LR}^2} - 1 \leq 0 \tag{1}$$

where

$$F = \frac{1}{2}\left(\frac{1}{(\sigma_{RR}^y)^2} + \frac{1}{(\sigma_{TT}^y)^2} - \frac{1}{(\sigma_{LL}^y)^2}\right),$$
$$G = \frac{1}{2}\left(\frac{1}{(\sigma_{TT}^y)^2} + \frac{1}{(\sigma_{LL}^y)^2} - \frac{1}{(\sigma_{RR}^y)^2}\right)$$
$$H = \frac{1}{2}\left(\frac{1}{(\sigma_{LL}^y)^2} + \frac{1}{(\sigma_{RR}^y)^2} - \frac{1}{(\sigma_{TT}^y)^2}\right),$$
$$L = \frac{3}{2(\sigma_{RT}^y)^2},\ M = \frac{3}{2(\sigma_{TL}^y)^2},\ N = \frac{3}{2(\sigma_{LR}^y)^2} \tag{2}$$

where σ_{ij} is the stress tensor and σ_{ij}^y is the yield stress.

The material constants of the metal washer and bolt were assumed as the mechanical properties of SS400, which is a steel grade defined in the Japanese Industrial Standard. The Young's modulus, Poisson's ratio, and yield stress of the metal washer and bolt were taken from the literature [18]. The wood had three Young's moduli, E_L, E_R, and E_T, three shear moduli, G_{LT}, G_{LR}, and G_{RT}, six Poisson's ratios, ν_{LT}, ν_{TL}, ν_{LR}, ν_{RL}, ν_{RT}, and ν_{TR}, and six yield stresses, $\sigma^y{}_L$, $\sigma^y{}_R$, $\sigma^y{}_T$, $\sigma^y{}_{LT}$, $\sigma^y{}_{LR}$, and $\sigma^y{}_{RT}$. The Young's modulus (E_R) and yield stress ($\sigma^y{}_R$) of the wood

in the radial direction were obtained from the compressive test performed by Matsubara et al. [11]. The Young's moduli in the other two directions and the shear moduli were calculated from E_R using the following relationships for coniferous forests [19]:

$$E_L{:}E_R{:}E_T = 22{:}2{:}1$$

$$G_{LR} : G_{LT} : G_{RT} = 20 : 17 : 1$$

$$E_L{:}G_{LR} = 16.7{:}1{:}1$$

The yield stresses in the other two directions were determined by considering the tensile and shear tests results of Japanese cedar [20], and it was assumed that $\sigma^y{}_T$ is equal to $\sigma^y{}_R$ and $\sigma^y{}_{LT}$ is equal to $\sigma^y{}_{LR}$ and $\sigma^y{}_{RT}$ as shown in previous studies [6, 12, 21]. The Poisson's ratio in each direction was obtained from the experimental results of Japanese cedar in literature [22]. The material constants of the bolt, metal washer, and wood are summarized in Tables 2 and 3, respectively. It should be noted that the assumptions of elastic modulus and yield stress were used conveniently; however, this may be inappropriate for some analyses which are sensitive to the material constants in each direction. Thus, the sensitivity of embedment behavior of this study to material constants was investigated as mentioned latter.

The three-dimensional FEA was carried out considering geometrical and material nonlinearity using Abaqus/Standard. The analysis was carried out sequentially on a single workstation with a dual 4-core CPU with a clock speed of 3.8 GHz and 96 GB RAM. The calculation time was approximately 24 h.

Results and discussion

Experimental results

As observed by Matsubara et al. [11], two types of deformation modes in the experiment were observed: the metal washer around the bolt hole partially bending and being embedded into the wood, and the entire metal washer being embedded into the wood. The former was observed in the washer with small thickness and long side length, i.e., low bending stiffness. The latter was observed in the washer with large thickness and short side length, i.e., high bending stiffness.

Comparison between experimental and numerical results

This section compares the embedment test results and FEA results. It should be noted that a few cases of FEA diverged during the equilibrium iteration. However, the numerical results could be compared with the experimental results without loss of generality, because FEA was performed beyond the yield load in all cases.

Figure 3 shows the embedment load–displacement curves obtained via the experiment and FEA for each side length of the metal washer. Table 4 lists the initial stiffness K and yield load P^y. The initial stiffness was obtained from the first straight line using the least-square methods, and

Table 2 Material constants of bolt and metal washer

E	ν	σ^y
205,000 MPa	0.3	235 MPa

Table 3 Material constants of wood

E_L:	1386 MPa	ν_{LT}:	0.58	$\sigma^y{}_L$:	71.4 MPa
E_R:	126 MPa	ν_{TL}:	0.0173	$\sigma^y{}_R$:	2.50 MPa
E_T:	63 MPa	ν_{LR}:	0.405	$\sigma^y{}_T$:	2.50 MPa
G_{LT}:	70.5 MPa	ν_{RL}:	0.0289	$\sigma^y{}_{LT}$:	5.20 MPa
G_{LR}:	83.0 MPa	ν_{RT}:	0.901	$\sigma^y{}_{LR}$:	5.20 MPa
G_{RT}:	4.15 MPa	ν_{TR}:	0.378	$\sigma^y{}_{RT}$:	5.20 MPa

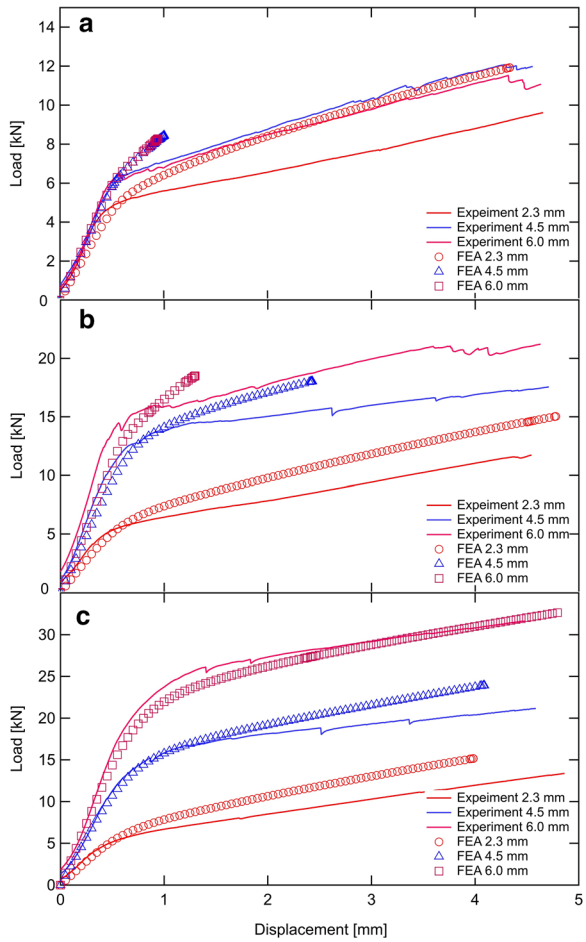

Fig. 3 Embedment load–displacement curves obtained via experiments and FEA. Side lengths of metal washers are (**a**) 40, (**b**) 60, and (**c**) 80 mm

Table 4 Initial stiffness and yield load obtained via experiment and FEA

Metal washer		*K* [kN/mm]			P^y [kN]		
Side length [mm]	Thickness [mm]	FEA	Exp	FEA/Exp	FEA	Exp	FEA/Exp
40	2.3	9.36	11.78	0.79	5.94	4.75	1.25
	4.5	11.82	14.49	0.82	7.11	6.29	1.13
	6.0	12.16	15.22	0.80	7.11	5.98	1.19
60	2.3	10.72	14.73	0.73	7.23	5.59	1.29
	4.5	19.31	23.10	0.84	13.79	13.84	1.00
	6.0	22.29	25.17	0.89	14.80	15.58	0.95
80	2.3	11.23	15.08	0.74	6.62	5.57	1.19
	4.5	22.56	25.00	0.90	16.17	15.14	1.07
	6.0	29.48	34.19	0.86	23.67	19.91	1.19

the yield load was defined as an intersection of first and second straight lines. In the experiment, the initial slip displacement occurred owing to the clearance between the upper surface of the nut and the steel plate jig. This clearance in the experiment cannot be dealt with by FEA. Because of this, the embedment load–displacement curve was intentionally translated along the *x*-axis to remove the clearance. The trends of the experimental load–displacement curves were broadly reproduced by the FEA. However, on average, the initial stiffness and yield load in the numerical results were 18% lower and 14% higher than those in the experimental results, respectively.

Figure 4 shows the residual displacement of wood after the embedment test is finished and the distribution of the equivalent plastic strain of wood at the final step of the FEA. In the case of the metal washer with a large thickness and a small side length (S40T6), the equivalent plastic strain of wood increased along the edge of the metal washer, because the metal washer had high bending stiffness and small bending deformation. By contrast, in the case of the metal washer with a small thickness and a large side length (S80T2.3), the plastic deformation of wood occurred in a wide area owing to the bending deformation of the metal washer. The trend of the plastic deformation of wood was also observed from the residual deformation in the experiment, where the area with high plastic strain approximately corresponded to the area with large residual deformation.

Figure 5 shows the development of the equivalent plastic strain of wood in cases S40T6 and S80T2.3 at two points, i.e., when the load reached the yield point and when plastic deformation increased after the yield point. In particular, the development of plastic deformation in the longitudinal and tangential directions is examined. In S40T6, the stress of wood was concentrated beneath the edge of the metal washer. At the yield point, plastic deformation was distributed in the diagonal direction from the edge of the metal washer on the RT (R: radial, T: tangential) symmetric plane. After the yield point, plastic deformation increased in the diagonal direction and along the edge of the metal washer. The side length and stiffness of wood in the longitudinal direction were higher than those in the tangential direction. Thus, the wood was deflected toward the tangential direction, as shown in Fig. 6. In addition, the plastic deformation of wood in the tangential direction preceded that in the longitudinal direction. During the loading process, the shape of the metal washer remained intact owing to its high bending stiffness. By contrast, in S80T2.3, the plastic deformation of wood was distributed around the bolt hole at the yield point, unlike S40T6, because the metal washer with low bending stiffness was deformed by the vertical force from the bolt and its center part compressed the wood. After the yield point, plastic deformation uniformly extended in the longitudinal and tangential directions; in particular, it increased in the tangential direction.

Sensitivity of embedment behavior to material constants

As discussed in the previous section, the embedment behavior of the metal washer into wood might be influenced by the mechanical properties in not only the radial direction but also the longitudinal and tangential directions. This section describes the numerical analysis of the sensitivity of embedment behavior to the material constants in each direction. In the analysis, the elastic modulus and yield stress of wood in cases S40T6 and S80T2.3 were intentionally doubled as compared with the original models. However, when $\sigma^y{}_T$ or $\sigma^y{}_R$ were doubled individually, the values of G and H in Eq. (2) became negative, which caused instability in the equilibrium iteration of the FEA. Thus, $\sigma^y{}_T$ and $\sigma^y{}_R$ were doubled simultaneously. A previous study reported that embedment behavior was insensitive to Poisson's ratio; hence, Poisson's ratio was not considered in the sensitivity analysis in this study [23]. The ratios of initial

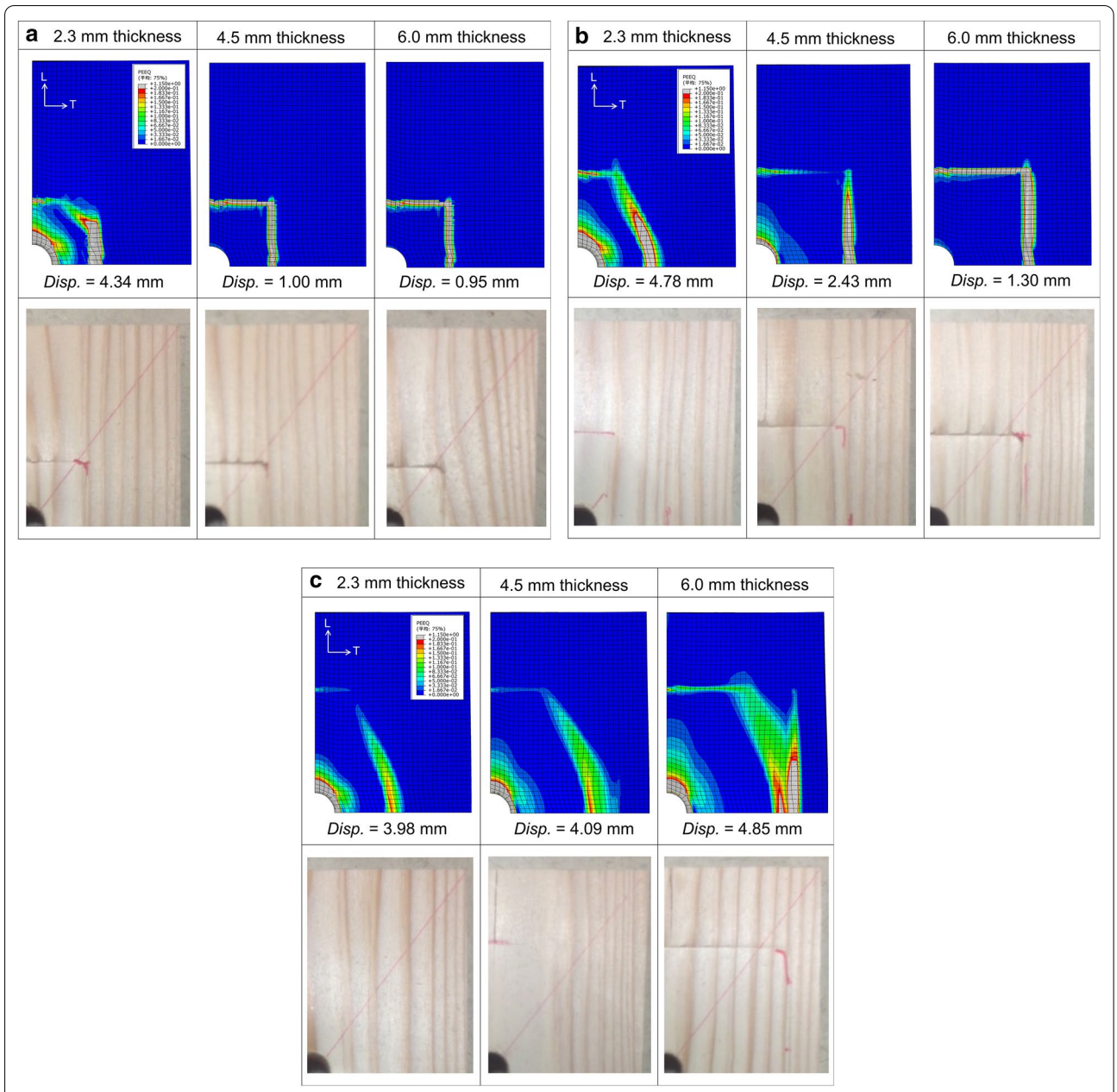

Fig. 4 Residual displacement of wood after embedment test is finished, and distribution of equivalent plastic strain of wood in the LT (L: longitudinal, T: tangential) plane at the final step of FEA. Side lengths of metal washers are (**a**) 40, (**b**) 60, and (**c**) 80 mm

stiffness K and yield load P^y with and without doubled material constants are defined as follows:

$$r^K = \frac{K \text{ in FEA with intentionally changed material constants}}{K \text{ in FEA without intentionally changed material constants}} \tag{4}$$

$$r^P = \frac{P^y \text{ in FEA with intentionally changed material constants}}{P^y \text{ in FEA without intentionally changed material constants}}. \tag{5}$$

Figures 7 and 8 show the embedment load–displacement curves obtained via the FEA with the intentionally changed elastic modulus and yield stress in each direction. r^K and r^P are listed in Table 5. K increased when E_R was doubled, K and P^y increased when E_T was doubled, and P^y increased when ${\sigma^y}_R$ and ${\sigma^y}_T$ were doubled. K and P^y were only slightly affected when the other elastic moduli and yield stresses were doubled. It was evident that E_R and ${\sigma^y}_R$ affected K and P^y because the radial direction

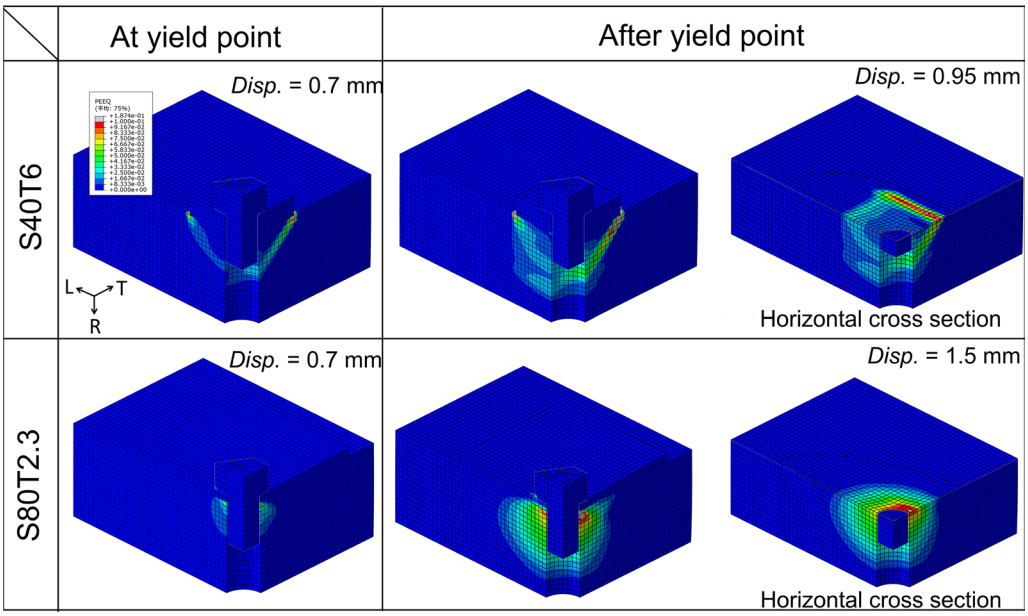

Fig. 5 Development of equivalent plastic strain in S40T6 and S80T2.3

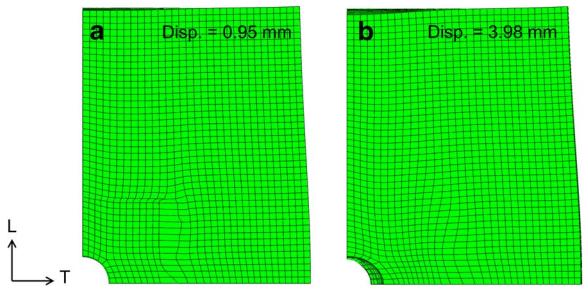

Fig. 6 Deformation of wood at final step in (**a**) S40T6 and (**b**) S80T2.3, whose scale is magnified 10 and 5 times, respectively (L: longitudinal, T: tangential)

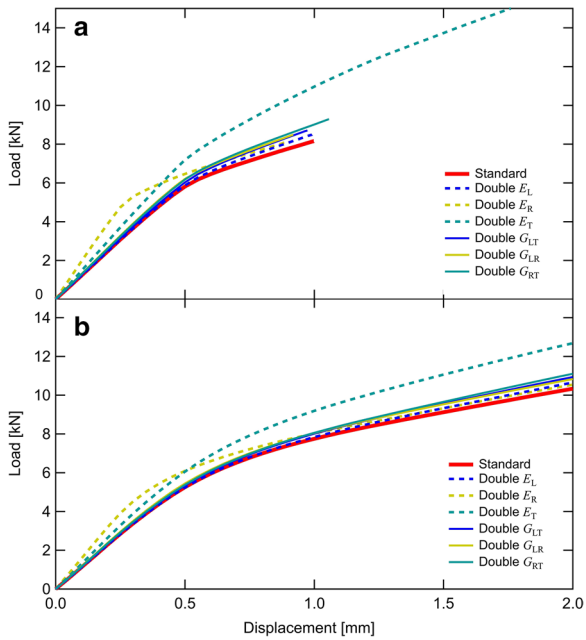

Fig. 7 Embedment load–displacement curves obtained via FEA with intentionally changed elastic moduli in (**a**) S40T6 and (**b**) S80T2.3

was parallel to the direction of vertical force. In addition, E_T and $\sigma^y{}_T$ influenced K and P^y owing to the large deflection of wood toward the tangential direction, as noted in the previous section. In S40T6, the maximum increase in K (approximately 30%) and P^y (approximately 90%) was observed when E_R was doubled and when $\sigma^y{}_R$ and $\sigma^y{}_T$ were simultaneously doubled, respectively. The influence of the intentionally changed elastic modulus and yield stress was stronger in S40T6 compared to S80T2.3 because the bending deformation of the metal washer affected K and P^y in S80T2.3. The results show that the measurement of E_T, E_R, $\sigma^y{}_T$, and $\sigma^y{}_R$ via material testing is important for reproducing the behavior of the embedment of the metal washer into wood and accurately estimating the yield load and initial stiffness using FEA.

Conclusions

The mechanism of the embedment behavior of a bolted joint was examined using FEA. A metal washer was embedded into wood in the radial direction. The numerical results were validated by comparing them

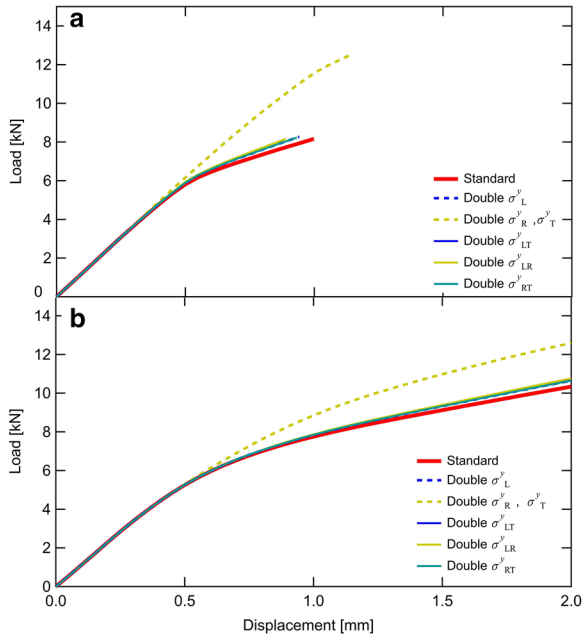

Fig. 8 Embedment load–displacement curve obtained via FEA with intentionally changed material constants in (**a**) S40T6 and (**b**) S80T2.3

with experimental results. In addition, the sensitivity of embedment behavior to the elastic modulus and yield stress of wood in each direction was investigated through numerical analysis. The major findings are as follows:

(1) The trends of the embedment load–displacement curves observed in the embedment tests were approximately reproduced by the FEA results. On average, the initial stiffness and yield load obtained via numerical analysis were 18% lower and 14% higher than those obtained via experiments, respectively. Moreover, the residual displacement of wood in the experiment approximately corresponded to the distribution of the equivalent plastic strain of wood in the FEA.

(2) In the numerical case of the metal washer with high bending stiffness, the plastic deformation of wood initiated beneath the edge of the metal washer and extended in the tangential direction mainly owing to the difference between the stiffness in the tangential and longitudinal directions. On the contrary, in the case of the metal washer with low stiffness, the plastic deformation of wood initiated in the vicinity of the bolt hole and then developed particularly in the tangential direction.

(3) The initial stiffness and yield load for the embedment were sensitive to the Young's modulus and yield stress of wood in the tangential and radial directions. The influence of the change in these material constants was stronger in the case of the metal washer with high bending stiffness compared to low bending stiffness. Thus, the measurement of these constants through material testing is important for reproducing the behavior of the embedment of a metal washer into wood and accurately estimating the yield load and initial stiffness using FEA.

In this study, the geometrical properties of the metal washer were varied for the experiment and FEA, whereas the geometrical properties of wood (Japanese cedar) were fixed; this might affect the embedment behavior. In future, the variation in the geometrical properties of wood should be considered to obtain general results.

Table 5 Ratio of initial stiffness and yield load before and after changing material constants

Model	Doubled constant	r^K	r^P	Doubled constant	r^K	r^P
S40T6	E_L	1.00	1.06	σ^y_L	1.00	1.05
	E_R	1.27	0.93	σ^y_R, σ^y_T	1.02	1.91
	E_T	1.21	1.46	–	–	–
	G_{LR}	1.06	1.11	σ^y_{LR}	1.01	1.05
	G_{LT}	1.01	1.11	σ^y_{LT}	1.01	1.05
	G_{RT}	1.05	1.11	σ^y_{RT}	1.01	1.05
S80T2.3	E_L	0.98	1.01	σ^y_L	1.00	1.01
	E_R	1.31	0.94	σ^y_R, σ^y_T	1.00	1.32
	E_T	1.15	1.20	–	–	–
	G_{LR}	1.02	1.05	σ^y_{LR}	1.00	1.01
	G_{LT}	1.02	1.05	σ^y_{LT}	1.00	1.01
	G_{RT}	1.01	1.05	σ^y_{RT}	1.00	1.01

Abbreviations
FEA: Finite-element analysis.

Acknowledgements
Not applicable.

Authors' contributions
TM carried out the finite-element analysis and investigated its results. DM designed and performed the experiments. YW, HS, and AK assisted in the preparation of the experiments. TM wrote the manuscript in consultation with DM, YW, HS, and AK. All authors read and approved the final manuscript.

Funding
This work was supported in part by grants from the Japan Society for the Promotion of Science (KAKENHI, JP19K06180).

Availability of data and materials
Not applicable.

Declarations

Ethics approval and consent to participate
Not applicable.

Consent for publication
We agree to allow the publication of our manuscript.

Competing interests
The authors declare that they have no competing interests.

Author details
[1]Niigata University, 8050, Ikarashi 2-no-cho, Nishi-ku, Niigata 950-2181, Japan. [2]Kindai University, 11-6 Kayanomori, Iizuka, Fukuoka 820-8555, Japan. [3]Toyama Prefectural Agricultural, Forestry and Fisheries Research Center, Imizu, Toyama 4940939-0311, Japan. [4]Sugiyama Jogakuen University, 17-3, Chikusa-ku, Nagoya, Aichi 464-8662, Japan. [5]Osaka Sangyo Univerisity, 3 Chome-1-1 Nakagaito, Daito, Osaka 574-8530, Japan.

Received: 19 March 2021 Accepted: 17 May 2021
Published online: 27 May 2021

References

1. Lathuillière D, Bléron L, Descamps T, Bocquet J-F (2015) Reinforcement of dowel type connections. Constr Build Mater 97:48–54
2. Nishiyama N, Ando N (2003) Analysis of load-slip characteristics of nailed wood joints: application of a two-dimensional geometric nonlinear analysis. J Wood Sci 49(6):505–512
3. Sawata K, Yasumura M (2003) Estimation of yield and ultimate strengths of bolted timber joints by nonlinear analysis and yield theory. J Wood Sci 49(5):383–391
4. Sawata K (2015) Strength of bolted timber joints subjected to lateral force. J Wood Sci 61(3):221–229
5. Gečys T, Bader TK, Olsson A, Kajėnas S (2019) Influence of the rope effect on the slip curve of laterally loaded, nailed and screwed timber-to-timber connections. Constr Build Mater 228:116702
6. A Awaludin, T Toshiro Hayashikawa, T Hirai, Y Sasaki. 2010 Loading resistance of bolted timber joints beyond their Yield-loads. In: Proceedings of the 2nd ASEAN Civil Engineering Conference, Vientiane
7. Wusqo U, Awaludin A, Irawati IS, Setiawan AF (2019) Study of laminated veneer lumber (LVL) sengon to concrete joint using two-dimensional numerical simulation. J Civ Eng Forum 5(3):275–288
8. Awaludin A, Hirai T, Hayashikawa T, Sasaki Y (2008) Load-carrying capacity of steel-to-timber joints with a pretensioned bolt. J Wood Sci 54(5):362–368
9. Awaludin A, Hirai T, Hayashikawa T, Sasaki Y, Oikawa A (2008) Effects of pretension in bolts on hysteretic responses of moment-carrying timber joints. J Wood Sci 54(2):114–120
10. Awaludin A, Hirai T, Sasaki Y, Hayashikawa T, Oikawa A (2011) Beam to column timber joints with pretensioned bolts. Civ Eng Dimens 13(2):59–64
11. Matsubara D, Shimada M, Hirai T, Funada R, Hattori N (2016) Embedment of metal washers into timber members of bolted timber joints I. Application of the theory of a beam on an elastic foundation. Mokuzai Gakkaishi 62(4):119–132
12. Awaludin A, Hirai T, Hayashikawa T, Leijten A (2012) A finite element analysis of bearing resistance of timber loaded through a steel plate. Civ Eng Dimens 14(1):1–6
13. Kuwamura H (2011) Coefficient of friction between wood and steel under heavy contact. J Struct Constr Eng 76(666):1469–1478
14. de Souza Neto EA, Peric D, Owen DR (2011) Computational methods for plasticity: theory and applications. Wiley, New York
15. Ambartsumian SA (1964) Theory of anisotropic shells. NASA IT F-118, Washington D.C.
16. Hill R (1948) A theory of the yielding and plastic flow of anisotropic metals. Proc R Soc A Math Phys Eng Sci 193(1033):281–297
17. Awaludin A, Irawati IS, Shulhan MA (2019) Two-dimensional finite element analysis of the flexural resistance of LVL Sengon non-prismatic beams. Case Stud Constr Mater 10:e00225
18. Architectural Institute of Japan (2017) AIJ design standard for steel structures: Based on allowable stress concept (2005 edition). Architectural Institute of Japan, Tokyo
19. Takahashi T, Nakayama Y (2015) Wood science series III. Physics. Kaisei-sha, Shiga
20. Kuwamura H (2013) Failure strength of wood in single-bolted joints loaded parallel-to-grain: Study on steel-framed timber structures, Part 16. J Struct Constr Eng 78(691):1575–1584
21. Sirumbal-Zapata LF, Málaga-Chuquitaype C, Elghazouli AY (2018) A three-dimensional plasticity-damage constitutive model for timber under cyclic loads. Comput Struct 195:47–63
22. Architectural Institute of Japan (2014) Fundamental theory of timber engineering. Architectural Institute of Japan, Tokyo
23. Mitsui S, Minami Y, Kawachi T, Kondo K (2010) Finite element analysis of wooden behavior of compressive strain inclined to the grain: (Part-1) Outline of the present approach and some numerical analyses of uniform partial compression test. J Struct Eng 56:359–369

Publisher's Note